

# Daily fluctuations propagate damply through the accretion disk of Swift J1727.8-1613

Han He<sup>1†</sup>, Yi Long<sup>2†</sup>, Bei You<sup>1</sup>, Fu-Guo Xie<sup>3</sup>, Zhen Yan<sup>3</sup>,  
Andrzej A. Zdziarski<sup>4</sup>, Sai-En Xu<sup>1</sup>

<sup>1</sup>Department of Astronomy, School of Physics and Technology, Wuhan University, Wuhan, 430072, Hubei, China.

<sup>2</sup>Department of Astronomy, Nanjing University, 163 Xianlin Avenue, Nanjing, 210023, Jiangsu, China.

<sup>3</sup>Shanghai Astronomical Observatory, Chinese Academy of Sciences, Shanghai, 200030, Shanghai, China.

<sup>4</sup>Nicolaus Copernicus Astronomical Center, Polish Academy of Sciences, Bartycka 18, PL-00-716, Warszawa, Poland.

<sup>†</sup>These authors contributed equally to this work.

## Abstract

Propagating fluctuations within accretion disks are known to induce multi-wavelength variability across diverse timescales. While these fluctuations have been widely invoked to explain rapid timing phenomena within the inner disk region in the frequency domain, observational signatures of outer-disk fluctuations propagating in the time domain remain sparse. Here, we present an analysis of observations by the Hard X-ray Modulation Telescope (HXMT) during the 2023 outburst of the newly discovered low-mass black hole X-ray binary Swift J1727.8–1613. Follow-up, high-cadence monitoring reveals intense variability in disk emission, attributable to fluctuations in the accretion rate. These disk fluctuations exhibit damped amplitudes and shortened flare periods. We interpret these features as observational evidence of fluctuations originating at and propagating from large radii, supported by fitting the disk light curves with a propagating fluctuation model. Furthermore, we propose that a plausible mechanism driving these fluctuations is the cyclical propagation of heating and cooling fronts in the context of the disk instability model. This work bridges theoretical predictions with time-domain observations, offering critical insights into the dynamic processes governing accretion disks.

**Keywords:** accretion, black hole, X-ray, fluctuation

## Introduction

Accreting compact objects—ranging from stellar-mass white dwarfs (WDs), neutron stars (NSs), and stellar-mass black holes (BHs) to supermassive BHs—exhibit multi-wavelength variability across various timescales. This variability is attributed to intrinsic fluctuations in the accretion disk [1–3]. Notably, fluctuations originating at a given disk radius propagate inward, imprinting variability characterized by the local high-frequency variation and low-frequency variation stirred up at and propagated from large radii [4–6]. Consequently, the observations of multi-timescale variability in systems such as cataclysmic variables (CVs; [7]), X-ray binaries (XRBs; [2, 8–10]), ultraluminous X-ray sources (ULXs; [11]), and active galactic nuclei (AGNs; [12]) constrains models of fluctuation propagation in disks, thereby probing the disk dynamics which are otherwise missed by spectral analysis.

The propagating fluctuation model is widely invoked to explain rapid timing phenomena, including flat-top noise in power density spectra (PDS) and multi-wavelength time lags [13, 14]. Previous studies have focused on high-frequency variability ( $\sim 10$ – $100$  Hz in XRBs to millihertz in AGNs) within the inner disk region ( $< 10^2 R_g$ ,  $R_g$  is the gravitational radius) [8, 13, 15–17]. However, observational evidence for outer-disk fluctuations propagating inward remains sparse, despite their critical role in understanding how the inner disk responds to variable mass accretion from outer regions. Here, we analyze the 2023 outburst of the black hole X-ray binary Swift J1727.8–1613 to identify long-timescale flux fluctuations propagating from the outer disk, likely driven by disk instabilities.

Swift J1727.8–1613 is a new low-mass black hole X-ray binary first identified by Swift/BAT on August 24, 2023 (MJD 60180) [18]. Subsequent follow-up observations were conducted by a sequence of instruments, including NICER, NuSTAR, and MAXI [19]. Recent optical observations derived a distance of  $d = 3.7 \pm 0.3$  kpc [20]. Dynamic analysis established a lower limit for the compact object’s mass of  $M_1 > 3.12 \pm 0.10 M_\odot$  and refined the parameters to  $P_{\text{orb}} = 0.45017 \pm 0.00004$  d [20]. In addition, the hard X-ray modulation telescope (HXMT) performed long-term, high-cadence follow-up observations from August 25, 2023 (MJD 60181), to October 6, 2023 (MJD 60223), capturing Swift J1727.8–1613 displaying a peak flux of 7 Crab in the 15–50 keV range, making it one of the brightest X-ray binary systems [21, 22]. Based on the spectral and timing analysis, Swift J1727.8–1613 remained in the state transition for 43 days between September 2, 2023 (MJD 60189) and October 15, 2023 (MJD 60232) [23–28]. This was corroborated by the Rms-Intensity Diagram (RID; see 1.2). During this long state transition, HXMT recorded a sequence of multiple flares in the low energy band and a relatively smooth decline in the high energy band [26], which indicates strong activity in the accretion disk [29].

## Disk flares

Figure 1 illustrates the light curve monitored by three instruments (LE: 2–4 and 4–10 keV; ME: 10–30 keV; HE: 30–100 keV) onboard HXMT (see Section 1.1 for data reduction). The date entering the state transition is marked with a red dashed line. We observe from the light curve that the variation is significantly greater in the LE band

compared to that in the ME and HE bands. Specifically, the LE light curve features a sequence of distinctive and intense flares between MJD 60197 and MJD 60223 with a flat global trend. To simplify, we have divided the multiple flares into five distinct epochs labeled as flares 1 through 5 (hereafter referred to as  $f_1$  to  $f_5$ ). These flares approximately span the time intervals: MJD 60197–MJD 60203, MJD 60203–MJD 60210, MJD 60210–MJD 60215, MJD 60215–MJD 60219, and MJD 60219–MJD 60221, as shaded in Figure 1.

We perform the spectral fits for the HXMT observations during the flaring phase between  $f_1$  and  $f_5$  (see Section 1.3). The disk luminosity  $L_{\text{disk}}$  and Compton luminosity  $L_{\text{Comp}}$ , estimated at a distance of  $d = 3.7$  kpc [20] (see Section 1.4 for more detail). The temporal evolutions are presented in Figure 2. The analysis reveals a highly variable disk component and a comparatively stable Compton component. Specifically, the disk luminosity exhibits significant variability, characterized by a sequence of damped multi-flares with decreasing periods superimposed on a weak upward trend. The reduction in peak luminosities from  $f_2$  to  $f_5$  suggests a damping of disk emission fluctuations, mirroring the trend observed in the LE light curve. In contrast, the Compton luminosity shows minimal flaring activity, except for a transient flare during  $f_1$ . Consequently, the Compton component initially dominates the observed LE flare during  $f_1$ , after which the disk emission becomes increasingly prominent. This variable disk emission further exhibits a dynamic, positive correlation between the photon index  $\Gamma$  and the Compton luminosity  $L_{\text{Comp}}$  (see Section 1.8). Spectral analysis indicates a quasi-stable inner disk radius extending to  $\sim 8R_g$ , implying that fluctuations in disk emission are primarily driven by variations in the inner accretion rate (see Section 1.4).

Critically, the inferred thermal disk extending close to the innermost stable circular orbit (ISCO) provides fundamental constraints on the origin of accretion rate variations. Local generation of such fluctuations at the inner disk is implausible, as the associated timescales (typically tens of seconds for a stellar-mass black hole [8, 13, 15–17]) are orders of magnitude shorter than the observed daily variability. We therefore propose that the observed disk emission variations likely originate from accretion rate fluctuations generated with progressively shortened periods at specific radii in the outer disk. These fluctuations propagate inward through the disk, gradually modifying the inner disk accretion rate while being naturally damped by viscous diffusion [30].

## Viscous damping in the accretion disk

To test this hypothesis, we analyze the observed disk flares within the framework of the propagating fluctuation model, accounting for the viscous diffusion on the propagation. The inner accretion rate in the framework of infinite disk can be analytically determined using Green functions if the outer modulation  $\dot{M}_0$  at a given radius  $R_0$  is provided [4, 5, 13, 30–32]. Given the quasi-stable inner disk radius during the flares, we approximate the disk luminosity as  $L_{\text{disk}} = \eta \dot{M}_{\text{in}} c^2$ , where  $\eta$  is assumed to be a constant. This enables a direct fit of the variation of the disk emission. Instead of modeling the overall variation of the disk luminosity, we focus on modeling four individual flares occurring between  $f_2$  and  $f_5$ , as highlighted in Figure 3. Mathematically the intrinsic

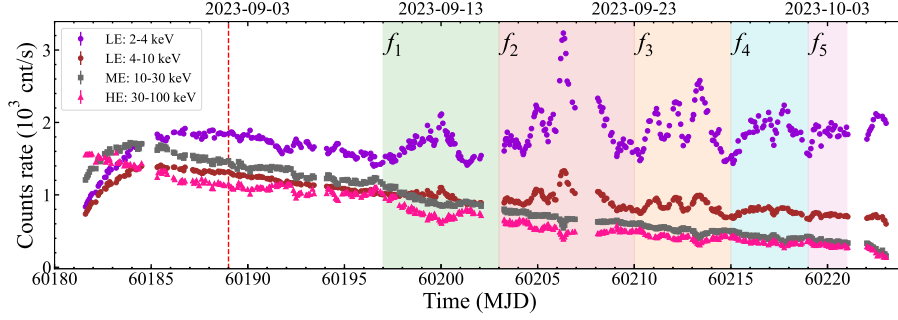


**Fig. 1** The X-ray light curve of Swift J1727.8-1613, as monitored by HXMT, is illustrated in the LE bands (2-4 keV in purple, 4-10 keV in brown), ME band (10-30 keV in grey), and HE band (30-100 keV in pink). The date entering the state transition is marked with a red dashed line. The shaded regions in green, red, orange, blue, and purple correspond to the phases  $f_1$  to  $f_5$ . Error bars are negligible and not visible for most data points. For visualization, the data in the ME and HE bands are scaled down by factors of 0.9 and 0.7, respectively.

oscillation of  $\dot{M}_0$ , i.e. fluctuations in the outer region of the disk, can be modeled as a sum of a series of cosinoidal functions. As the accretion mass propagates inwards, viscous diffusion progressively damps the amplitude of the fluctuations [30]. We then apply these functions to fit the disk variability using the Markov chain Monte Carlo (MCMC) sampler implemented in the `emcee` package in `Python` [33] (see Section 1.5). We try one, two, and three cosinoidal functions to  $\dot{M}_0$ , and find that single or double cosinoidal functions are insufficient to reproduce the triple-peaked light curve during each phase. Below we focus on the modelling based on three cosinoidal functions of  $\dot{M}_0$ . The fitting results demonstrate strong agreement with the disk light curve (see Figure 3), accurately capturing its key features, including the damped amplitude and reduced flare periods.

We then study the fitting parameters of the propagating fluctuation model. The evolutions of main parameters, including the local viscous timescale  $t_{\text{visc}}(R_0)$ , flare periods  $P$ , and amplitudes of three cosinoidal functions  $A_i$  are presented in Figure 4. We find the local viscous timescale remains approximately constant at  $t_{\text{visc}}(R_0) = 0.66$  days within the uncertainty. This corresponds to a radial coordinate of  $R_0 = 2000R_g (\alpha/0.2)^{2/3}$ , based on the thermal and viscous timescales in the standard thin disk model [34] (see Section 1.6). The exponential parameters for stellar-mass BHXRBs of  $H/R = 0.02$  [34] and  $M_{\text{BH}} = 10M_\odot$  are used in the calculation. The viscous parameter  $\alpha$  was suggested to be in the range of 0.2-1 according to the numerical simulation [35]. This derives a large radii of  $R_0 \geq 2000R_g$ , corresponding to  $R_0 = 3 \times 10^9$  cm for a  $10M_\odot$  BH. However, it is important to note that  $R_0$  does not represent the radius where fluctuations originate but rather the radius at which external fluctuations propagate. This is due to the derived local viscous timescale  $t_{\text{visc}}(R_0)$  being significantly smaller than the flare periods  $P$  (i.e., timescales of fluctuation). In general,  $P$  is considered to be of the order of the local viscous timescale in the propagating fluctuation model, suggesting the fluctuations are generated at a larger radius than  $R_0$ . Additionally, the fluctuation period decreases linearly from

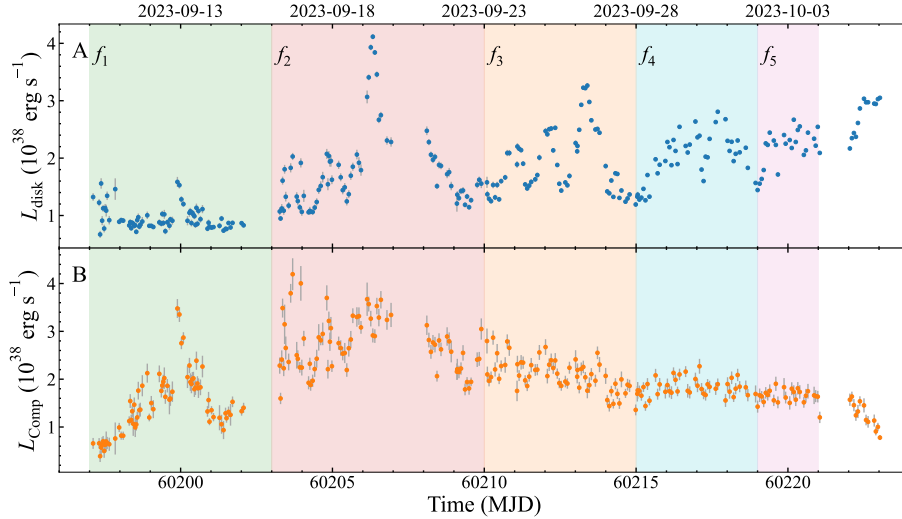


**Fig. 2** The luminosity evolution for the spectral components in 0.01-1000 keV is shown. Panel A presents the disk luminosity  $L_{\text{disk}}$  consisting of the intercepted  $L_{\text{seed}}$  and observed photons, whereas Panel B illustrates the Compton luminosity  $L_{\text{Comp}}$ . The shaded regions in green, red, orange, blue, and purple correspond to the phases  $f_1$  to  $f_5$ .

5.3 days to 2.5 days. Combined with the quasi-steady viscous timescale, this suggests an increase in the ratio  $t_{\text{visc}}(R_0)/P$ , thereby enhancing viscous damping [30]. Consequently, the amplitude of fluctuations in  $\dot{M}_{\text{in}}$  and  $L_{\text{disk}}$  diminishes over time as  $t_{\text{visc}}(R_0)/P$  increases. Furthermore, the derived parameters  $A_i$  remain nearly constant within uncertainties, indicating a stable external fluctuation source. This confirms that the observed damped amplitude arises from viscous diffusion through the disk rather than the intrinsically diminishing external fluctuation source. Therefore, the results support the hypothesis that the variations of the disk emission are modulated by propagating fluctuations originating in the outer disk. These fluctuations propagate through the disk and become detectable upon reaching  $R_0$ . As the period shortens, the viscous damping strengthens over time, progressively reducing the amplitude of the accretion rate and, consequently, the disk luminosity.

## Plausible mechanism for the disk flares

The next issue is how these fluctuations are generated in the outer disk. Magneto-hydrodynamic (MHD) turbulence, driven by processes such as the magnetorotational instability [36, 37], is hypothesized to act as the primary mechanism for generating the fluctuations in the accretion disk. However, such fluctuations arise on millisecond timescales in the inner disk region [2, 4, 8, 13, 17, 32], i.e., much shorter than the daily timescale variability observed in this study.

One plausible mechanism for these daily fluctuations is the disk instability model (DIM) [38, 39]. When the instability is triggered, a density spike propagates outward

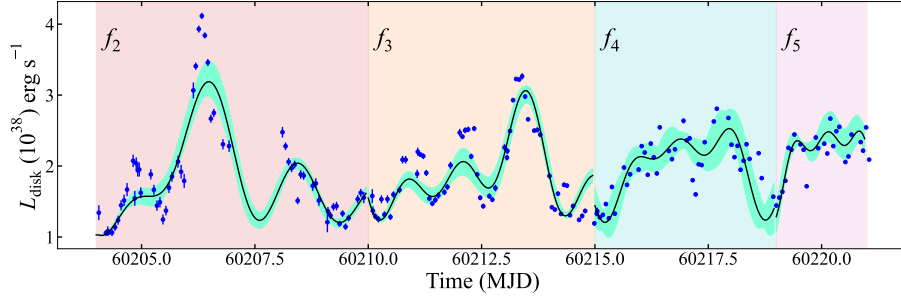


**Fig. 3** The fits to the disk flares from  $f_2$  to  $f_5$  using the propagating fluctuation model, assuming the disk inner radius is constant. The blue dots represent the luminosity of the seed photons from the disk, while the black line illustrates the outcomes derived from the median values of free parameters in the propagating fluctuation model (see Figure 4). The green shaded region indicates the uncertainties at  $1\text{-}\sigma$  level. Additionally, the red, yellow, blue, and purple shaded regions correspond to the periods associated with  $f_2$ ,  $f_3$ ,  $f_4$ , and  $f_5$ , respectively.

along the temperature gradients, resulting in the formation of a heating front. The propagation speed depends on the viscosity parameter  $\alpha$  and the sound speed  $c_S$  [39–41]. This outward propagation persists until the density of the post-front drops below the minimum threshold permitted by the hot branch, at which point a cooling front initiates and propagates inward. The interplay between these two fronts governs the observed flare, with the rising phase linked to the outward-moving heating front and the decay phase associated with the inward-moving cooling front [39, 42]. Throughout the decay phase, the surface density remains below the maximum allowable value on the cold branch, influenced by factors such as irradiation and disk winds [42–44]. However, if the surface density behind the cooling front exceeds the maximum value, the cooling front transitions into a heating front [39, 42]. This generates a sequence of fluctuations also referred as “reflares” in ref. [39], which has been numerically studied [42, 43, 45–47]. For instance, simulation of a stellar-mass BH reveals the fluctuations, which is the result of the cyclic propagation of heating and cooling fronts between  $4 \times 10^4 R_g$  to  $7.5 \times 10^4 R_g$  [42].

However, to date, no observational evidence for fluctuations has been found in either dwarf or X-ray binaries [39, 48]. The characteristics of the disk variability of Swift J1727.8-1613 exhibit strong similarity to those of the fluctuations, suggesting this might be the first observational detection of the fluctuations. More specifically, the propagation speed of these fronts depends on the viscosity parameter  $\alpha$  and the sound speed  $c_S$  [39–41]. If assuming  $\alpha = 0.2$  and  $c_S = 10 \text{ km/s}$  (the front temperature is  $\sim 10^4 \text{ K}$  due to the hydrogen being ionized [39, 43]), we derive a 5.8 days outward-backward propagation cycle between  $R = 4 \times 10^4 R_g$  and  $R = 7.5 \times 10^4 R_g$  (see Section 1.7). The derived timescale of cyclic propagation aligns closely with the flare periods, implying the disk variability observed in Swift J1727.8-1613 originates from the disk instability in the outer region.

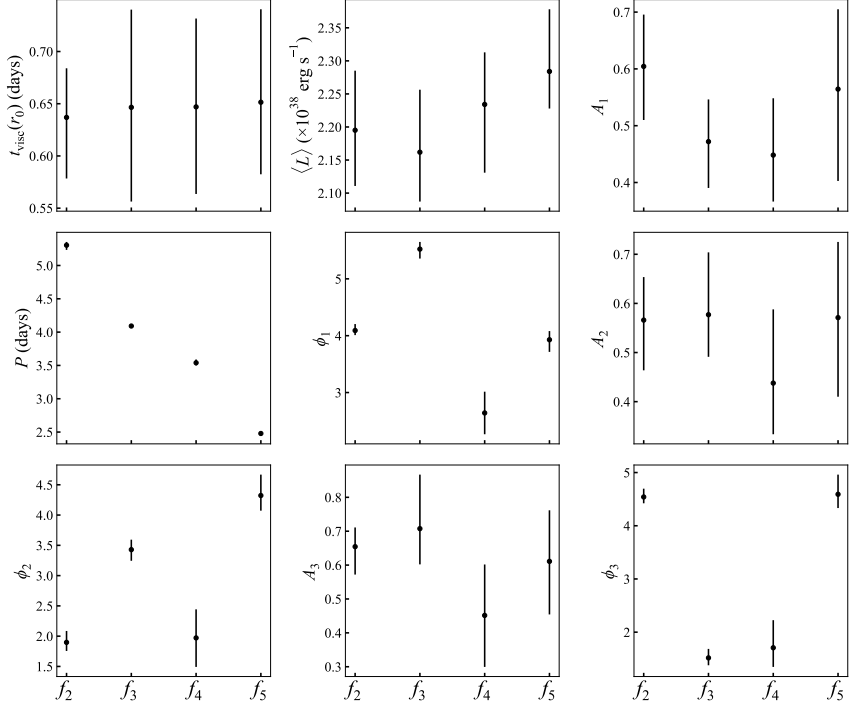


**Fig. 4** The evolution of the free parameters in the propagating fluctuation model. The dots represent the median values for each parameter. The uncertainties are quoted at 1- $\sigma$  level.

## Conclusion

In this study, we investigate the variable disk emission characterized by the damped amplitude and shortened modulation period, in the 2023 outburst of the newly discovered low-mass black hole X-ray binary Swift J1727.8-1613. These disk fluctuations further modulate the seed photons for Comptonization, driving a dynamic  $\Gamma - L_{\text{Comp}}$  relation. For the first time, we report observational evidence that the observed disk flares are caused by the accretion rate fluctuations in the outer disk, which most likely originate from the fluctuations predicted by the accretion disk instability model. The viscous damping during the fluctuation propagation through the disk governs the damped amplitude. This hypothesis is further validated by directly fitting the observed disk flares with the propagating fluctuation model.

# Methods

## 1.1 HXMT data reduction

HXMT consists of three telescopes: Low Energy X-ray Telescope (LE, 1-15 keV), Medium Energy X-ray Telescope (ME, 5-30 keV), and High Energy X-ray Telescope (HE, 20-250 keV). LE contains three detector boxes, and each box contains 32 CCD, which is a kind of Swept Charge Device (SCD), leading to a total detection area of 952 cm<sup>2</sup>. HE uses 1728 Si-PIN detectors with a total detection area of 952 cm<sup>2</sup>. HE is composed of 18 cylindrical NaI(Tl)/CsI(Na) phoswich detectors with a total detection area of 5000 cm<sup>2</sup> (see The Insight-HXMT Data Reduction Guide for details). Fluorescence lines due to the photoelectric effect of electrons in Silver K-shell are detected by the Si-PIN detectors of ME, which dominate the spectra over 21–24 keV. Hence, the spectra over 21–24 keV are ignored. According to the calibration tests since its launch, the chosen energy bands in this work are 2-10 keV for LE, 10-30 keV for ME, and 30-100 keV for HE, with a systematic error of 1.5% for three instruments [49].

We use the Insight-HXMT Data Analysis software (HXMTDAS, v2.06) for the data reduction, filtering the data with the default configuration <sup>1</sup>. The joint spectra overlapped by three instruments are extracted by screening the event files for different good time intervals (GTIs). For the GTIs with short exposure, we combine these close GTIs to improve the signal-to-noise ratio of spectra. For simplicity, we selected the ME GTIs as the input of the screening events, as the time range of GTIs in ME encompasses that in LE and HE for most observations. Then, we get all the spectra separated by the ME GTIs for the analysis.

## 1.2 Basic diagrams and timing analysis

The three diagrams, the hardness-intensity diagram (HID), RMS-intensity diagram (RID), and the hardness-RMS diagram (HRD) are useful for investigating the evolution of the outburst and identifying the spectral states [50]. The RMS used in RID is integrated over a broad range of frequencies in the power density spectra (PDS) [50]. Therefore, we used the `powspec` package in HEASoft to compute the PDS for each observation made by HXMT in detectors, using a 64 s interval and a corresponding 1/128 s time resolution. After subtracting Poisson noise, the PDS is normalized using the Miyamoto normalization [51]. The diagrams are plotted in Figure 5. Here, the intensity is the count rate in the 1-10 keV. The hardness ratio is defined as the ratio of the count rate in the 3-10 keV to that in the 1-3 keV. The RMS is integrated over a broad frequency range of 0.1-60 Hz in PDS. The source began the outburst at the bottom right of the HID and then moved to the upper left. Meanwhile, in the RID, a diagonal line extending from the lower left to the upper right indicates that the source is in the hard state [50]. Subsequently, the deviations from the diagonal line indicate that the source entered the state transition around MJD 60188. These results are consistent with the criterion based on QPO evolution [28].

---

<sup>1</sup><http://hxmtweb.ihep.ac.cn/SoftDoc/847.jhtml>



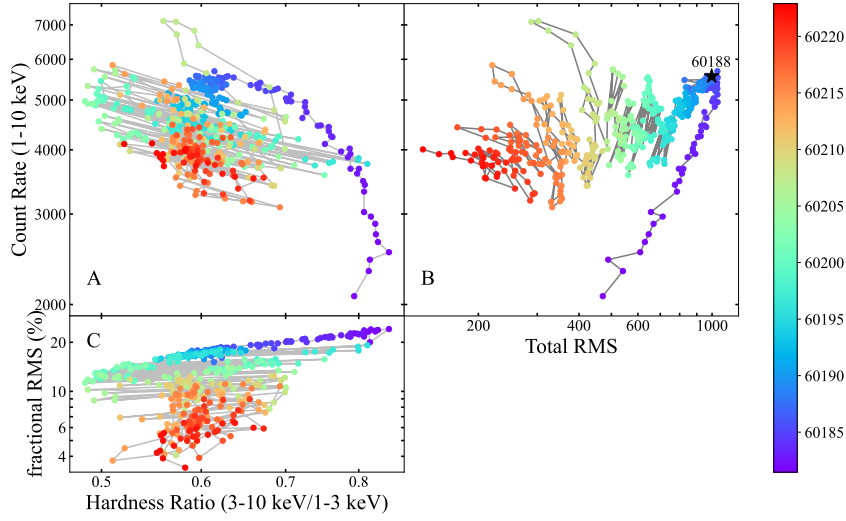


**Fig. 5** Swift J1727.8-1613 outburst diagrams observed with HXMT: (A) Hardness-Intensity Diagram (HID); (B) RMS-Intensity Diagram (RID); (C) Hardness-RMS Diagram (HRD). The black star indicates the onset of the hard-to-soft state transition. The error bars are negligible for most data points, and the color of each point corresponds to the time of observation.

### 1.3 Spectral analysis

In the spectral fitting, a systematic error of 1.5% is added to data [49]. The spectra are analyzed using the model `constant*tbabs*(thcomp⊗diskbb+relxillCp)` in XSPEC version 12.13.0 [52]. The `tbabs` model [53] represents the Galactic absorption with the fixed column density of  $N_{\text{H}} = 0.226 \times 10^{22} \text{ cm}^{-2}$  [54]. The `thcomp` model describes the spectra from Comptonization by thermal hot electrons [55]. The `diskbb` model accounts for the disk thermal emission. The `relxillCp` model is the relativistic reflection model containing both the direct emission from the corona and its reflection on the disk [56]. We assume the iron abundance  $A_{\text{Fe}} = 1.0$  in solar units and the inclination  $\theta = 40^\circ$  [19]. The reflection fraction  $R_{\text{f}}$  is defined in the rest frame as the ratio of intensity emitted towards the disk compared to escaping to infinity, and we set  $R_{\text{f}} = -1$  to obtain the reflected component [57]. The outer radius of the reflection disk is fixed at the upper limit of their table model  $R_{\text{out}} = 1000R_{\text{g}}$ , where  $R_{\text{g}} = GM/c^2$  is the gravitational radius. The input inner radius in `relxillCp` model is linked to the normalization in `diskbb`, which directly relates to the true inner disk radius as the ref [58, 59]:

$$N_{\text{diskbb}} = \frac{(R'_{\text{in}}/1 \text{ km})^2 \cos \theta}{(d/10 \text{ kpc})^2}. \quad (1)$$

Here,  $R'_{\text{in}}$  is the apparent inner radius,  $\theta$  is the inclination, and  $d$  is the distance. The intrinsic inner radius  $R_{\text{in}}$  relates to the observed apparent one  $R'_{\text{in}}$  as  $R_{\text{in}} = \kappa^2 \zeta R'_{\text{in}}$ , where we adopt the color correction factor  $\kappa = 1.7$  for a diluted blackbody [60]. The parameter  $\zeta$  accounts for the inner boundary condition correction. According to [58],  $\zeta \simeq 0.41$  is applied to the case of a non-spinning black hole with a disk extending to ISCO. Although the black hole in Swift J1727.8-1613 likely has a spin of  $a > 0$  [19, 26], it remains unclear if the inner disk reaches the ISCO or not during the state transition. Therefore, we adopt  $\zeta = 1$  to neglect the effect of this factor in this work.

The disk temperature is predominantly high, ranging from 0.6-1.0 keV, with damped oscillations centered around  $\sim 0.9$  keV between  $f_2$  and  $f_5$ . The variation is most pronounced during  $f_2$ , i.e., it rises from 0.6 keV to 1.0 keV and then drops to  $\sim 0.65$  keV and additionally has several minor peaks. Subsequently,  $T_{\text{in}}$  ascends to 1.0 keV again and then descends to 0.75 keV, presenting the most distinct minor peaks, which correspond with the fluctuations observed in  $L_{\text{disk}}$  during  $f_3$ . Beyond this, the minor peaks become diminished, settling at  $\sim 0.9$  keV during  $f_4$  and  $f_5$ .

#### 1.4 Evolution of the accretion thin disk

The intrinsic disk flux  $F_{\text{disk}}$  and X-ray Comptonization flux  $F_{\text{Comp}}$  in 0.01-1000 keV are estimated using task **cflux** in **XSPEC**.  $F_{\text{disk}}$ , composed of the seed photons for Compton cooling and the unscattered soft photons, is directly estimated through **diskbb** model. The flux estimated by **thcomp** contains the flux of the Comptonized photons and the unscattered soft photons from the disk [55]. Therefore, given the covering fraction  $c_f$ , the flux of the seed photons for Compton cooling  $F_{\text{seed}}$  and the Comptonization flux  $F_{\text{Comp}}$  can be estimated as  $F_{\text{seed}} = c_f F_{\text{disk}}$  and  $F_{\text{Comp}} = F_{\text{thcomp}} - (F_{\text{disk}} - F_{\text{seed}}) = F_{\text{thcomp}} - (1 - c_f) F_{\text{disk}}$ , respectively [55]. The disk and Compton luminosities are then calculated at a distance of  $d = 3.7$  kpc.

The disk component exhibits significant variability, manifested in a sequence of damped multi-flares against a background of a slight upward trend. The disk luminosity was initially subdued during phase  $f_1$ , causing a minor change in flux. The disk emissions between  $f_2$  and  $f_5$  show significant X-ray flux modulation throughout the transition, which underwent temporal evolution characterized by a dampened amplitude and a shortened modulation period, resembling the LE light curve. The most intense disk flare at  $f_2$  increased the luminosity to  $4.12 \times 10^{38} \text{ erg s}^{-1}$ , a  $\sim 4.37$ -fold increase. The disk flare during  $f_3$  showed the most distinct structure, with a peak luminosity of  $1.74 \times 10^{38} \text{ erg s}^{-1}$ , increasing from the minimum by a factor of  $\sim 2.72$ . During  $f_4$ , the peak luminosity of the disk flare reached  $1.65 \times 10^{38} \text{ erg s}^{-1}$ ,  $\sim 2.55$  times above the minimum. During  $f_5$ , the peak luminosity was measured at  $1.43 \times 10^{38} \text{ erg s}^{-1}$ , a  $\sim 1.85$ -fold rise. The decrease in peak luminosities and the diminished variability from  $f_2$  to  $f_5$  suggest a damping of disk emission fluctuations, mirroring the LE light curve trend. Notably, the duration of the flares also decreased, from 7 days during  $f_2$  to 2 days during  $f_5$ , implying a reduction in the modulation period.

On the other hand, the Compton luminosity does not exhibit significant multiple flares similar to the disk emission but included a transient flare period during  $f_1$ . Following this, the Compton luminosity rose until MJD 60206 before it gradually decreased to approximately  $4.18 \times 10^{37} \text{ erg s}^{-1}$ .

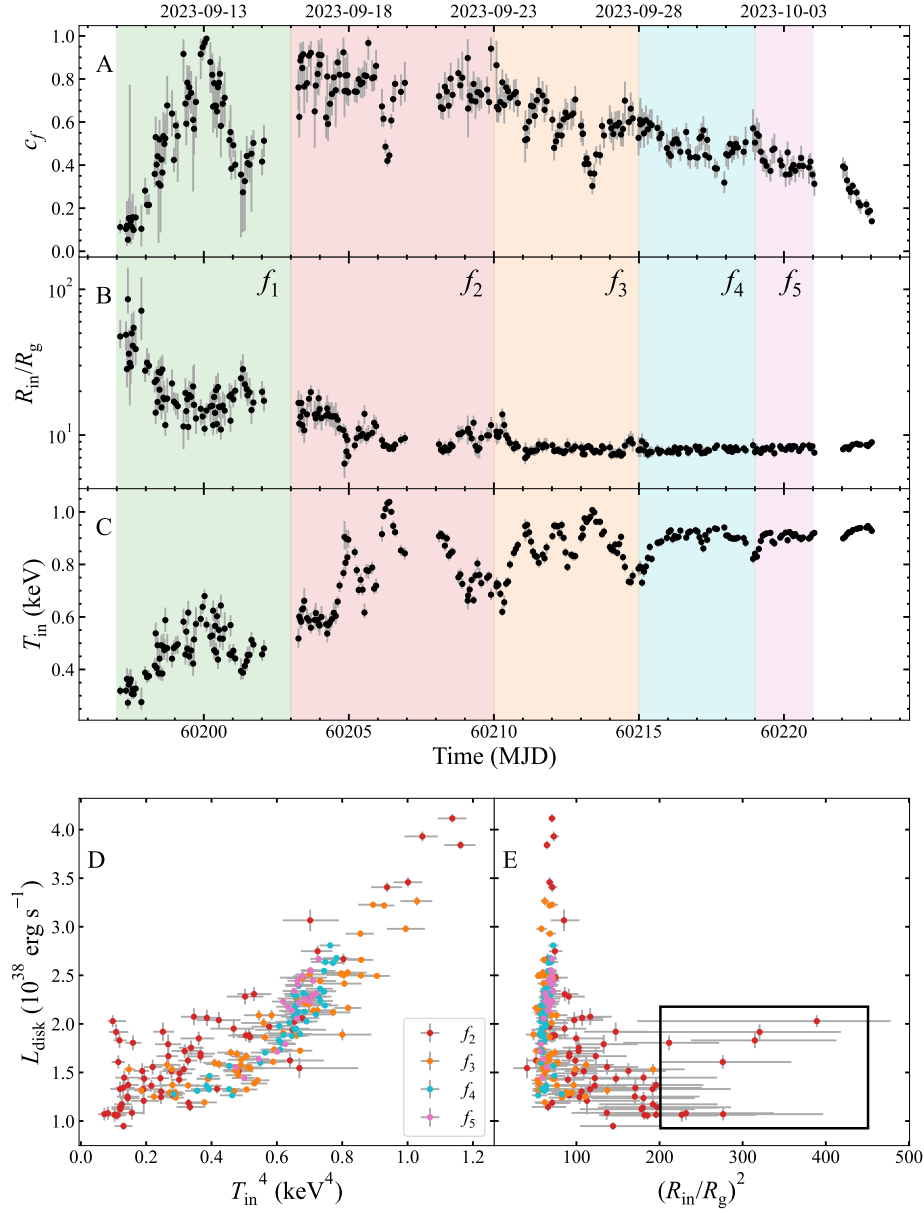


**Fig. 6** Panel A to C: Temporal Evolution of the parameters estimated from the spectral fitting: A) the disk temperature at the inner radius  $T_{in}$ ; B) the inner radius  $R_{in}$  in units of  $R_g$ ; C) the covering fraction  $c_f$ . Panel D to E: Correlations between disk luminosity  $L_{disk}$  and  $T_{in}$  and  $R_{in}$  respectively. The green, red, yellow, blue, and purple shaded regions and points represent periods  $f_1$  through  $f_5$ , respectively.

According to the description of `diskbb`, the disk emission can be estimated by a simplified scaling relation of  $L_{\text{disk}} \propto T_{\text{in}}^4 R_{\text{in}}^2$ , where  $R_{\text{in}}$  is the inner disk radius and  $T_{\text{in}}$  is the corresponding temperature at this boundary. In this work, the temperature  $T_{\text{in}}$  is measured directly from the spectral analysis, while the inner disk radius  $R_{\text{in}}$  is estimated from the normalization in `diskbb` (see Equation 1). The temporal evolutions of  $T_{\text{in}}$  and  $R_{\text{in}}$  are plotted in Figures 6 B and C. We find that the disk temperature is predominantly high, ranging from 0.6–1.0 keV, with damped oscillations centered around  $\sim 0.9$  keV between  $f_2$  and  $f_5$ . Concurrently, the inner radius  $R_{\text{in}}$  undergoes slight fluctuations before stabilizing around  $8 R_g$  from  $f_2$  to  $f_5$ , indicating a thermal disk extending into the strong gravity regime within a few gravitational radii. Thus, the observed damped variations in disk emission are hypothesized to stem from oscillations in  $T_{\text{in}}$  rather than the quasi-stable  $R_{\text{in}}$ . This interpretation is strongly supported by the distinct temperature dependence of  $L_{\text{disk}}$ , as shown in Figure 6D. We find a robust correlation with Spearman’s coefficient  $r_S = 0.87$  (significance  $> 99.9\%$ ), whereas the  $L_{\text{disk}} - R_{\text{in}}^2$  relation remains statistically marginal ( $r_S = -0.32$  at  $4.7\sigma$  level, see Figure 6E). These results unambiguously identify temperature modulation as the principal driver of disk emission variability. Furthermore, since `diskbb` neglects the inner boundary assuring  $T_{\text{in}} = 0$  at the ISCO,  $T_{\text{in}}$  can be expressed as a function of the mass accretion rate  $\dot{M}$  and the inner disk radius  $R_{\text{in}}$ , following the formula of  $T_{\text{in}} \propto (\dot{M}/R_{\text{in}}^3)^{1/4}$ . Given the quasi-stable  $R_{\text{in}}$  as observed, it can be inferred that it is the accretion rate dominating the temperature variations and thereby generating the fluctuation in the disk emission.

### 1.5 Fits with the propagating fluctuation model

The response of the inner disk to a changing accretion rate in its outer part has been investigated under different initial boundary assumptions using the propagating fluctuation model [30, 31, 61–64]. In our framework, we adopt a semi-infinite disk configuration extending radially to infinity, where a localized fluctuation emerges at finite radius  $R_0$ . The resultant inner accretion rate in the framework of infinite disk can be analytically determined using Green functions if the outer modulation  $\dot{M}_0$  at a given radius  $R_0$  is provided [4, 13, 30–32]. This can be expressed as

$$\dot{M}_{\text{in}}(\tau) = \int_0^\infty \dot{M}_0(\tau - \tau_1) G_{\dot{M}}(\tau_1) d\tau_1, \quad (2)$$

where  $G_{\dot{M}}(\tau)$  is the Green’s function at disk inner edge,  $\tau = t/t_{\text{visc}}(R_0)$  and  $t_{\text{visc}}(R_0)$  is the viscous timescale at  $R_0$ .

It should be noted that  $R_{\text{in}}$  exhibits exceptionally large uncertainties (see black rectangle in Figure 6E) during the MJD 60203–60204, making the temporal evolution of the accretion rate statistically unconstrained. Consequently, data during this period have been excluded in the subsequent analysis, as the severe parameter degeneracies between  $R_{\text{in}}$  and  $\dot{M}$  preclude reliable physical interpretation of the observed variations. Specifically, for each flare, the accretion rate at a given radius  $R_0$  is expressed using

three cosinoidal functions:

$$\dot{M}_0 = \langle \dot{M} \rangle \left[ 1 + \sum_{i=1}^3 A_i \cos \left( \frac{2\pi t}{P_i} + \phi_i \right) \right], \quad A_i \in [0, 1), \quad (3)$$

for  $60204 \leq t \leq 60221$ . Here  $\langle \dot{M} \rangle$ ,  $A_i$ ,  $P_i$ , and  $\phi_i$  represent the average accretion rate, modulation amplitude, period, and phase for each flare, respectively. We assume the relation  $P = P_1 = 2P_2 = 3P_3$ , which accounts for the sub-harmonic modulation. For the quiescent phases preceding MJD 60204 and following MJD 60221, where no significant fluctuations are observed,  $\dot{M}_0$  is set to the average rate between MJD 60197 and MJD 60204, and between MJD 60222 and MJD 60223, respectively. This assumption introduces a negligible impact on the results due to the low integrated contributions in these intervals. Using Eq. 2, we compute  $\dot{M}_{\text{in}}$  based on the expression for  $\dot{M}_0$  in Eq. 3. For simplicity, we assume  $L_{\text{disk}} = \eta \dot{M}_{\text{in}} c^2$ , where  $\eta$  is assumed to be a constant, given the quasi-stable inner disk radius during the flares. This enables a direct fit of the variation of the disk emission. More specially, the variable disk emission is fitted by

$$L = \int_0^\infty L_0(\tau - \tau_1) G_{\dot{M}}(\tau_1) d\tau_1, \quad (4)$$

$$L_0 = \langle L \rangle \left[ 1 + \sum_{i=1}^3 A_i \cos \left( \frac{2\pi i}{P} t + \phi_i \right) \right], \quad A_i \in [0, 1), \quad (5)$$

$$G_{\dot{M}}(\tau) = \frac{(2\mu^2)^2}{\Gamma(\mu)} \tau^{-1-\mu} \exp \left( -\frac{2\mu^2}{\tau} \right), \quad (6)$$

where

$$L_0 = \eta \dot{M}_0 c^2, \quad \tau \equiv \frac{t}{t_{\text{visc}}(R_0)}$$

$$P = P_1 = 2P_2 = 3P_3, \quad \mu = \frac{1}{4 - 2n}.$$

Here,  $L_0$  represents the power of the fluctuation at  $R_0$ . We adopt  $n = 3/5$  in the fitting, representing a thin disk supported by gas pressure and dominated by electron scattering [30].

We then apply Equations 4 to 6 to fit the disk variability using an MCMC sampler implemented in the `emcee` package in `Python` [33]. The free parameters include  $t_{\text{visc}}$ ,  $\langle L \rangle$ ,  $A_1$ ,  $P$ ,  $\phi_1$ ,  $A_2$ ,  $\phi_2$ ,  $A_3$ , and  $\phi_3$ . We initialized an ensemble of 100 walkers randomly distributed around the input values. The sampler was advanced for  $N = 5000$  steps, with the first 500 steps discarded as burn-in to ensure chains reach stationarity. To mitigate autocorrelation effects, we apply a thinning factor of 20 and flatten the chains to obtain a flat list of samples. This yielded 22500 independent posterior samples. We then estimate the median values and uncertainties quoted at the  $1-\sigma$  level (68% confidence interval) for each parameter.

## 1.6 The location of the original fluctuation

Based on the thermal and viscous timescales in the standard thin disk model [34], the radial coordinate of  $R_0$  in the modeling of the propagating fluctuations can be estimated using:

$$\begin{aligned} t_{\text{visc}}(R) &\approx t_{\text{th}} \left( \frac{H}{R} \right)^{-2} \\ &= 1.68 \left( \frac{\alpha}{0.01} \right)^{-1} \left( \frac{M_{\text{BH}}}{10M_{\odot}} \right) \left( \frac{R}{200R_g} \right)^{3/2} \left( \frac{H/R}{0.01} \right)^{-2} \text{ days,} \end{aligned} \quad (7)$$

where  $t_{\text{th}}$  is the thermal timescale, and  $H$  is the semi-thickness of the disk at  $R$ . We adopt a exponential parameters of  $H/R = 0.02$  [34] and  $M_{\text{BH}} = 10M_{\odot}$ . Substituting  $t_{\text{visc}}(R_0) = 0.66$  days into Equation 7, the radial coordinate of  $R_0$  can be expressed as:

$$R_0 \approx 2000R_g \left( \frac{\alpha}{0.2} \right)^{\frac{2}{3}} \quad (8)$$

The  $\alpha$ -viscosity parameter was suggested to be in the range of 0.2-1 in black hole XRBs [35]. If  $\alpha = 0.2$  is adopted,  $R_0 = 2000R_g$ , corresponding to  $\sim 3 \times 10^9$  cm for a typical stellar-mass BH with  $M_{\text{BH}} = 10M_{\odot}$ .

## 1.7 The timescale of the propagating fronts

The propagation speed of these fronts depends on the viscosity parameter  $\alpha$  and the sound speed  $c_S$  [39–41], which is

$$V_{\text{front}} \approx \alpha c_S. \quad (9)$$

Given the radial extent of the moving front, the characteristic duration of a flare can be derived by

$$t_{\text{front}} = \frac{\Delta R}{V_{\text{front}}} \approx \frac{\Delta R}{\alpha c_S}. \quad (10)$$

Substituting  $\Delta R = 3 \times 10^4 R_g$  into Equation 10, the characteristic front propagation timescale, corresponding to half the fluctuation period, exhibits a linear dependence on black hole mass through the relation:

$$t_{\text{front}} \approx \frac{\Delta R}{V_{\text{front}}} = \frac{3 \times 10^4 R_g}{\alpha c_S} = 0.29 \frac{M_{\text{BH}}}{M_{\odot}} \text{ days.} \quad (11)$$

Therefore, for  $M_{\text{BH}} = 10M_{\odot}$  of Swift J1727.8-1613, the fluctuation period is 5.8 days.

While the DIM has been extensively validated in explaining outbursts in CVs, NSXRBs, and BHXRBs, observational confirmation of disk instabilities in AGNs remains elusive. The findings on viscous damping of variability presented here are also applicable to accretion disks around supermassive black holes (SMBHs) in AGNs. Recent studies have reported AGN variability on timescales of decades [65, 66], suggesting that the variability patterns and underlying mechanisms identified in this work

may provide a framework to interpret such observations in SMBHs. This could show how the inner regions of AGN accretion disks respond to fluctuations in the mass supply rate originating from their outer regions.

## 1.8 The photon index-flux relation

It is well established that there is a correlation between the photon index  $\Gamma$  and X-ray luminosity  $L_X$  [67–70]. Below 1-2 percent of the Eddington luminosity  $L_{\text{Edd}}$ ,  $L_X$  shows a negative correlation with  $\Gamma$ . In contrast, luminous sources exhibit a positive correlation between  $\Gamma$  and  $L_X$ .

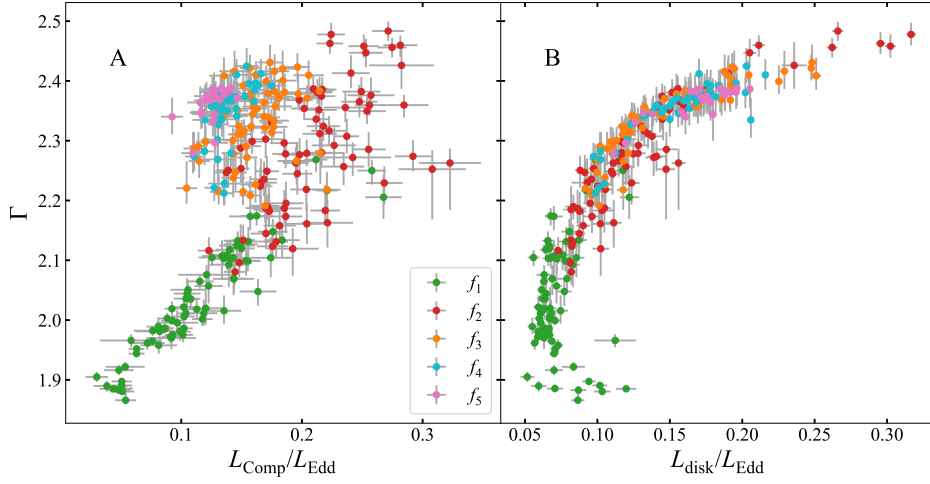
Figure 7A presents the correlation between the photon index  $\Gamma$  and the Compton luminosity  $L_{\text{Comp}}$ , scaled to the Eddington luminosity, from phases  $f_1$  to  $f_5$ . The green, red, orange, blue, and pink data points represent  $f_1$  to  $f_5$ , respectively. Notably,  $\Gamma$  is positively correlated with  $L_{\text{Comp}}$  during each flare, aligning with previous findings in this high-luminosity range. From  $f_2$  to  $f_5$ , Figure 7A illustrates a dynamic correlation between the photon index  $\Gamma$  and  $L_{\text{Comp}}$ . Specifically, the positive correlation shifts towards the upper left of the plane, characterized by a reduced range in both  $\Gamma$  and  $L_{\text{Comp}}$ . The relation between the Eddington scaled disk luminosity  $L_{\text{disk}}$  and  $\Gamma$  is also plotted in Figure 7B, exhibiting a significant positive relationship with a Spearman’s coefficient of  $r_S = 0.96$  at a confidence level of  $> 99.9\%$ .

Previous work attributed this positive correlation to the faster increase in the power of soft seed photons  $L_{\text{soft}}$  than the power supplied to the electrons in the hot accretion flow  $L_{\text{hard}}$  [70, 71]. Specifically, when the power supplied to the electrons in the hot accretion flow  $L_{\text{hard}}$  is fixed, an increase in the power of soft seed photons  $L_{\text{soft}}$  enhances Compton cooling, resulting in a softer energy spectrum [71]. Consequently, the photon index  $\Gamma$  positively correlates with the power ratio  $L_{\text{soft}}/L_{\text{hard}}$ . In the case of the soft seed photons originating from the accretion disk around BH,  $\Gamma$  can be estimated using [72],

$$\Gamma = \frac{7}{3}(A - 1)^{-\frac{1}{6}}, \quad (12)$$

where  $A = L_{\text{hard}}/L_{\text{soft}}$  represents the Compton amplification factor. Thus, the  $\Gamma - L_{\text{Comp}}$  correlation can be directly understood by analyzing the relationship between  $L_{\text{soft}}/L_{\text{hard}}$  and  $L_{\text{hard}}$ . In the following section, we apply this framework to interpret the observed dynamic  $\Gamma - L_{\text{Comp}}$  correlation depicted in Figure 7.

First, it is essential to estimate both  $L_{\text{hard}}$  and  $L_{\text{soft}}$ . Given the high Eddington ratio  $L_{\text{Comp}}/L_{\text{Edd}}$  in this study (Figure 7A), nearly all the energy absorbed by electrons in the hot accretion flow is efficiently radiated away [73]. This justifies the estimation of the Compton luminosity  $L_{\text{Comp}}$  as  $L_{\text{hard}}$  [70], i.e.,  $L_{\text{Comp}} \approx L_{\text{hard}}$ . Additionally, in the regime of bright X-ray luminosity, it is hypothesized that the soft seed photons for Compton cooling originate from the accretion disk [70]. However, equating  $L_{\text{disk}}$  directly with  $L_{\text{soft}}$  would be inaccurate, as not all soft photons are scattered due to the geometrical effects of the hot accretion flow. Through spectral fitting, we derive the evolution of the covering fraction  $c_f$ . Consequently, if the contribution from self-absorbed synchrotron emission in the hot flow is disregarded, the soft seed photons for Compton cooling can be approximated as  $L_{\text{soft}} \approx L_{\text{seed}} = L_{\text{disk}} \cdot c_f$ .



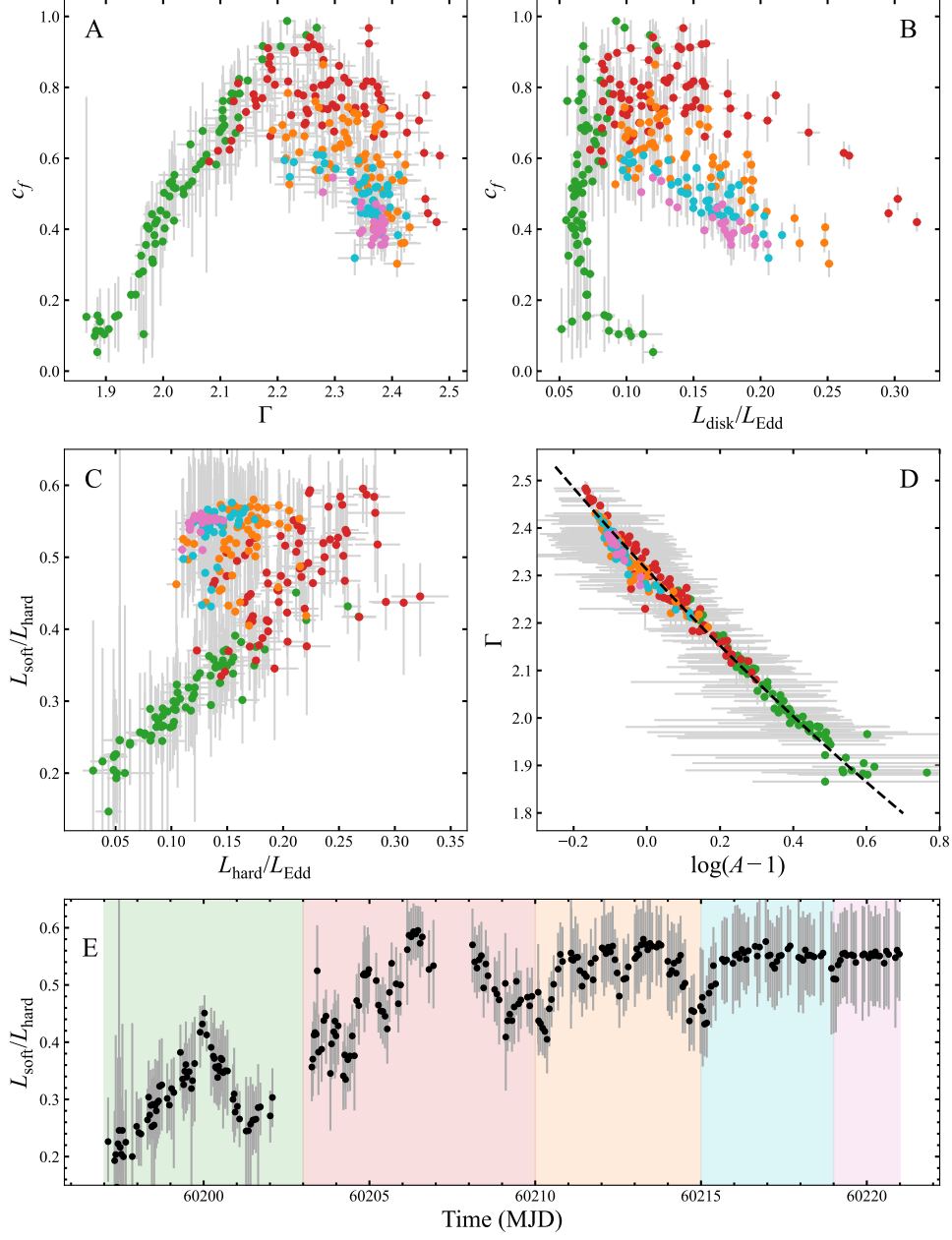
**Fig. 7** The relationship between the photon index  $\Gamma$  and Eddington-scaled Compton luminosity (left panel) and disk luminosity (right panel). The green, red, orange, blue, and pink dots represent the data points from phases  $f_1$  to  $f_5$ , respectively.

Figure 8A and B present the correlations between  $c_f$  and  $\Gamma$  and  $L_{\text{disk}}$ . It is inferred that the increase of Gamma at low  $L_{\text{disk}}$  are driven almost entirely due to increasing  $c_f$  at a near constant  $L_{\text{disk}}$ . As for higher  $L_{\text{disk}}$ , while  $c_f$  decreases,  $L_{\text{disk}}$  increases even more significantly, leading to a net softening of the spectrum. Figure 8C illustrates the correlation between  $L_{\text{soft}}/L_{\text{hard}}$  and  $L_{\text{Comp}}/L_{\text{Edd}}$ . A clear positive correlation is observed for each flare, indicating that  $L_{\text{soft}}$  increases more rapidly than  $L_{\text{hard}}$ . Based on the analysis in the literature [71],  $\Gamma$  is expected to exhibit a positive correlation with  $L_{\text{Comp}}$ . Additionally, we examine the relationship between  $\Gamma$  and  $A$ , as shown in Figure 8D. The spectral results exhibit excellent agreement with the theoretical framework proposed in the literature [72] within the uncertainties.

Furthermore, Figure 7A demonstrates a dynamic correlation from  $f_2$  to  $f_5$ , where positive correlations shift toward the upper left of the plane, characterized by a reduced range in  $\Gamma$ . According to Eq. 12, the variability in  $L_{\text{disk}}$  (i.e.,  $L_{\text{soft}}$ ), combined with the mild decrease in  $L_{\text{Comp}}$ , drives the changes in  $L_{\text{soft}}/L_{\text{hard}}$  (see Figure 8E), resulting in the observed dynamic  $\Gamma - L_{\text{Comp}}$  relationship. Additionally, viscous damping in the fluctuations of  $L_{\text{disk}}$  weakens the modulation in  $L_{\text{soft}}$ , thereby reducing the range of  $L_{\text{soft}}/L_{\text{hard}}$  and suggesting a narrowing range in  $\Gamma$ . Concurrently, the global increase in  $L_{\text{soft}}/L_{\text{hard}}$  indicates a higher  $\Gamma$ . As  $L_{\text{Comp}}$  decreases, the  $\Gamma - L_{\text{Comp}}$  relation shifts toward the upper left of the plane, accompanied by narrowing ranges in both  $\Gamma$  and  $L_{\text{Comp}}$ .

**Acknowledgements.** We thank Guillaume Dubus, Bi-Fang Liu, Xinwu Cao, Mouyuan Sun, Yue Wu, Di-Zhan Du, and Yi-Long Wang for their helpful discussions and comments. This work is supported by NSFC grants 12322307, 12273026,





**Fig. 8** A: The correlation between  $c_f$  and  $\Gamma$ ; B: The correlation between  $c_f$  and  $L_{\text{disk}}/L_{\text{Edd}}$ ; C: The correlation between  $L_{\text{soft}}/L_{\text{hard}}$  and Eddington scaled Compton luminosity  $L_{\text{Comp}}/L_{\text{Edd}}$ . D: The relation between the photon index  $\Gamma$  and the Compton amplification factor. The dashed line represents the best-fitting result; E: The temporal evolution of  $L_{\text{soft}}/L_{\text{hard}}$ . The green, red, yellow, blue, and purple shaded regions correspond to the periods from  $f_1$  to  $f_5$ , respectively. The colored dots here are the same as the ones in Figure 7.

12361131579, 12373049, 12192223, 12373017, and 12192220; by the National Program on Key Research and Development Project 2021YFA0718500; Xiaomi Foundation / Xiaomi Young Talents Program. F.G.X. is also supported by the National SKA Program of China (No. 2020SKA0110102), and 100101 Key Laboratory of Radio Astronomy and Technology (Chinese Academy of Sciences). Andrzej A. Zdziarski acknowledges support from the Polish National Science Center under the grants 2019/35/B/ST9/03944 and 2023/48/Q/ST9/00138.

**Data availability.** All Insight-HXMT data used in this work (Proposal ID: P0614338) are publicly available and can be downloaded from the Insight-HXMT website (<http://hxmt.org/> or <http://www.hxmt.cn/>).

**Author contributions.** B.Y. initiated the project and led the manuscript writing. H.H. led the modelling of the propagating fluctuation, and contributed to the text writing. Y.L. led to the spectral fits, and contributed to the text writing. F.-G. X. and Z. Y. wrote the code of the propagating fluctuation and contributed to the text writing. A. Z. contributed to the spectral fits and the text writing. S.-E. X contributed to the spectral fits. All the authors joined the discussion and the modification of the text at all stages.

## References

- [1] Ulrich, M.-H., Maraschi, L., Urry, C.M.: Variability of Active Galactic Nuclei. *Annual Review of Astronomy and Astrophysics* **35**, 445–502 (1997) <https://doi.org/10.1146/annurev.astro.35.1.445>
- [2] Done, C., Gierliński, M., Kubota, A.: Modelling the behaviour of accretion flows in X-ray binaries. Everything you always wanted to know about accretion but were afraid to ask. *The Astronomy and Astrophysics Review* **15**(1), 1–66 (2007) <https://doi.org/10.1007/s00159-007-0006-1> [arXiv:0708.0148](https://arxiv.org/abs/0708.0148) [astro-ph]
- [3] Padovani, P., Alexander, D.M., Assef, R.J., De Marco, B., Giommi, P., Hickox, R.C., Richards, G.T., Smolčić, V., Hatziminaoglou, E., Mainieri, V., Salvato, M.: Active galactic nuclei: what’s in a name? *The Astronomy and Astrophysics Review* **25**(1), 2 (2017) <https://doi.org/10.1007/s00159-017-0102-9> [arXiv:1707.07134](https://arxiv.org/abs/1707.07134) [astro-ph.GA]
- [4] Lyubarskii, Y.E.: Flicker noise in accretion discs. *Monthly Notices of the Royal Astronomical Society* **292**(3), 679–685 (1997) <https://doi.org/10.1093/mnras/292.3.679>
- [5] Frank, J., King, A., Raine, D.J.: *Accretion Power in Astrophysics: Third Edition*, (2002)
- [6] Uttley, P., Cackett, E.M., Fabian, A.C., Kara, E., Wilkins, D.R.: X-ray reverberation around accreting black holes. *The Astronomy and Astrophysics Review*

- 22**, 72 (2014) <https://doi.org/10.1007/s00159-014-0072-0> arXiv:1405.6575 [astro-ph.HE]
- [7] Hameury, J.-M., Lasota, J.-P.: VY Sculptoris stars as magnetic cataclysmic variables. *Astronomy and Astrophysics* **394**, 231–239 (2002) <https://doi.org/10.1051/0004-6361:20021136> arXiv:astro-ph/0207084 [astro-ph]
  - [8] Ingram, A., Done, C.: Modelling variability in black hole binaries: linking simulations to observations. *Monthly Notices of the Royal Astronomical Society* **419**(3), 2369–2378 (2012) <https://doi.org/10.1111/j.1365-2966.2011.19885.x> arXiv:1108.0789 [astro-ph.HE]
  - [9] Nixon, C., Salvesen, G.: A physical model for state transitions in black hole X-ray binaries. *Monthly Notices of the Royal Astronomical Society* **437**(4), 3994–3999 (2014) <https://doi.org/10.1093/mnras/stt2215> arXiv:1311.2930 [astro-ph.HE]
  - [10] Lucchini, M., Ten Have, M., Wang, J., Homan, J., Kara, E., Adegoke, O., Connors, R., Dauser, T., Garcia, J., Mastroserio, G., Ingram, A., van der Klis, M., König, O., Lewin, C., Mallick, L., Nathan, E., O’Neill, P., Panagiotou, C., Piotrowska, J., Uttley, P.: Variability as a Predictor for the Hard-to-soft State Transition in GX 339-4. *The Astrophysical Journal* **958**(2), 153 (2023) <https://doi.org/10.3847/1538-4357/ad0294> arXiv:2310.07462 [astro-ph.HE]
  - [11] King, A., Lasota, J.-P., Middleton, M.: Ultraluminous X-ray sources. *New Astronomy Reviews* **96**, 101672 (2023) <https://doi.org/10.1016/j.newar.2022.101672> arXiv:2302.10605 [astro-ph.HE]
  - [12] Ricci, C., Trakhtenbrot, B.: Changing-look active galactic nuclei. *Nature Astronomy* **7**, 1282–1294 (2023) <https://doi.org/10.1038/s41550-023-02108-4> arXiv:2211.05132 [astro-ph.GA]
  - [13] Mushtukov, A.A., Ingram, A., van der Klis, M.: Propagating mass accretion rate fluctuations in X-ray binaries under the influence of viscous diffusion. *Monthly Notices of the Royal Astronomical Society* **474**(2), 2259–2276 (2018) <https://doi.org/10.1093/mnras/stx2872> arXiv:1707.07578 [astro-ph.HE]
  - [14] Ingram, A.R., Motta, S.E.: A review of quasi-periodic oscillations from black hole X-ray binaries: Observation and theory. *New Astronomy Reviews* **85**, 101524 (2019) <https://doi.org/10.1016/j.newar.2020.101524> arXiv:2001.08758 [astro-ph.HE]
  - [15] King, A.R., Pringle, J.E., West, R.G., Livio, M.: Variability in black hole accretion discs. *Monthly Notices of the Royal Astronomical Society* **348**(1), 111–122 (2004) <https://doi.org/10.1111/j.1365-2966.2004.07322.x> arXiv:astro-ph/0311035 [astro-ph]
  - [16] Uttley, P., McHardy, I.M., Vaughan, S.: Non-linear X-ray variability in X-ray

- binaries and active galaxies. *Monthly Notices of the Royal Astronomical Society* **359**(1), 345–362 (2005) <https://doi.org/10.1111/j.1365-2966.2005.08886.x> [arXiv:astro-ph/0502112](#) [astro-ph]
- [17] Zhan, Y., You, B., Ingram, A., Jiang, W., Wang, F.: Modeling fast X-ray variability around an accreting black hole. *arXiv e-prints*, 2502–03995 (2025) [arXiv:2502.03995](#) [astro-ph.HE]
  - [18] Negoro, H., Serino, M., Nakajima, M., Kobayashi, K., Tanaka, M., Soejima, Y., Kudo, Y., Mihara, T., Kawamuro, T., Yamada, S., Tamagawa, T., Kawai, N., Matsuoka, M., Sakamoto, T., Sugita, S., Hiramatsu, H., Nishikawa, H., Yoshida, A., Tsuboi, Y., Urabe, S., Nawa, S., Nemoto, N., Shidatsu, M., Takahashi, I., Niwano, M., Sato, S., Higuchi, N., Yatsu, Y., Nakahira, S., Ueno, S., Tomida, H., Ishikawa, M., Ogawa, S., Kurihara, T., Ueda, Y., Setoguchi, K., Yoshitake, T., Nakatani, Y., Yamauchi, M., Hagiwara, Y., Umeki, Y., Otsuki, Y., Yamaoka, K., Kawakubo, Y., Sugizaki, M., Iwakiri, W.: MAXI/GSC detection of a new hard X-ray transient Swift J1727.8-1613 (GRB 230824A). *The Astronomer’s Telegram* **16205**, 1 (2023)
  - [19] Peng, J.-Q., Zhang, S., Shui, Q.-C., Zhang, S.-N., Kong, L.-D., Chen, Y.-P., Wang, P.-J., Ji, L., Qu, J.-L., Tao, L., Ge, M.-Y., Chang, Z., Li, J., Li, Z.-s., Yu, Z.-L., Yan, Z.: NICER, NuSTAR, and Insight-HXMT Views to the Newly Discovered Black Hole X-Ray Binary Swift J1727.8-1613. *The Astrophysical Journal Letters* **960**(2), 17 (2024) <https://doi.org/10.3847/2041-8213/ad17ca>
  - [20] Mata Sánchez, D., Torres, M.A.P., Casares, J., Muñoz-Darias, T., Armas Padilla, M., Yanes-Rizo, I.V.: Dynamical confirmation of a black hole in the X-ray transient Swift J1727.8-1613. *Astronomy and Astrophysics* **693**, 129 (2025) <https://doi.org/10.1051/0004-6361/202451960> [arXiv:2408.13310](#) [astro-ph.HE]
  - [21] Palmer, D.M., Parsotan, T.M.: Swift J1727.8-1613 reaches 7.6 Crab with strong QPO in Hard X-rays. *The Astronomer’s Telegram* **16215**, 1 (2023)
  - [22] Zhao, Q.-C., Tao, L., Li, H.-C., Zhang, S.-N., Feng, H., Ge, M.-Y., Ji, L., Wang, Y.-N., Huang, Y., Ma, X., Zhang, L., Qu, J.-L., Xu, Y.-J., Zhang, S., Yin, Q.-Q., Shui, Q.-C., Ma, R.-C., Zhao, S.-J., Li, P.-P., Yang, Z.-X., Liu, H.-X., Yu, W.: The First Polarimetric View on Quasiperiodic Oscillations in a Black Hole X-Ray Binary. *The Astrophysical Journal Letters* **961**(2), 42 (2024) <https://doi.org/10.3847/2041-8213/ad1e6c> [arXiv:2401.08970](#) [astro-ph.HE]
  - [23] Katoch, T., Antia, H.M., Nandi, A., Shah, P.: Detection of QPO in the peak of outburst of black hole candidate Swift J1727.8-1613: AstroSat/LAXPC Observation in Slow Mode. *The Astronomer’s Telegram* **16235**, 1 (2023)
  - [24] Katoch, T., Nandi, A., Shah, P.: Discovery detection of strong QPO at hard X-rays with AstroSat during ‘unusual’ peak of black hole transient Swift J1727.8-1613. *The Astronomer’s Telegram* **16243**, 1 (2023)

- [25] Mereminskiy, I., Lutovinov, A., Molkov, S., Krivonos, R., Semena, A., Sazonov, S., Tkachenko, A., Sunyaev, R.: Hard X-rays and QPO in Swift J1727.8-1613: the rise and plateau of the 2023 outburst. arXiv e-prints, 2310–06697 (2023) <https://doi.org/10.48550/arXiv.2310.06697> arXiv:2310.06697 [astro-ph.HE]
- [26] Yu, W., Bu, Q.-C., Zhang, S.-N., Liu, H.-X., Zhang, L., Ducci, L., Tao, L., Santangelo, A., Doroshenko, V., Huang, Y., Yang, Z.-X., Qu, J.-L.: Timing analysis of the newly discovered black hole candidate Swift J1727.8-1613 with Insight-HXMT. *Monthly Notices of the Royal Astronomical Society* **529**(4), 4624–4632 (2024) <https://doi.org/10.1093/mnras/stae835> arXiv:2403.13127 [astro-ph.HE]
- [27] Trushkin, S.A., Bursov, N.N., Nizhelskij, N.A., Tsybulev, P.G.: Bright radio flare from the X-ray binary Swift J1727.8-1613. *The Astronomer’s Telegram* **16289**, 1 (2023)
- [28] Mata Sánchez, D., Muñoz-Darias, T., Armas Padilla, M., Casares, J., Torres, M.A.P.: Evidence for inflows and outflows in the nearby black hole transient Swift J1727.8–162. *Astronomy and Astrophysics* **682**, 1 (2024) <https://doi.org/10.1051/0004-6361/202348754> arXiv:2401.04107 [astro-ph.HE]
- [29] Cao, J.-Y., Liao, J.-Y., Zhang, S.-N., Feng, H., Qu, J.-L., Zhang, L., Liu, H.-X., Yu, W., Zhao, Q.-C., Peng, J.-Q., Ge, M.-Y., Tao, L., Xu, Y.-J., Zhang, S., Yang, Z.-X.: Spectral analysis of the X-ray flares in the 2023 outburst of the new black binary transient Swift J1727.8–1613 observed with Insight-HXMT. arXiv e-prints (2025) <https://doi.org/10.48550/arXiv.2503.05411> . arXiv:2503.05411 [astro-ph]. Accessed 2025-03-10
- [30] Zdziarski, A.A., Kawabata, R., Mineshige, S.: Viscous propagation of mass flow variability in accretion discs. *Monthly Notices of the Royal Astronomical Society* **399**(3), 1633–1640 (2009) <https://doi.org/10.1111/j.1365-2966.2009.15386.x> arXiv:0902.4530 [astro-ph.HE]
- [31] Lynden-Bell, D., Pringle, J.E.: The evolution of viscous discs and the origin of the nebular variables. *Monthly Notices of the Royal Astronomical Society* **168**, 603–637 (1974) <https://doi.org/10.1093/mnras/168.3.603>
- [32] Kotov, O., Churazov, E., Gilfanov, M.: On the X-ray time-lags in the black hole candidates. *Monthly Notices of the Royal Astronomical Society* **327**(3), 799–807 (2001) <https://doi.org/10.1046/j.1365-8711.2001.04769.x> arXiv:astro-ph/0103115 [astro-ph]
- [33] Foreman-Mackey, D., Hogg, D.W., Lang, D., Goodman, J.: `emcee`: The mcmc hammer. *Publications of the Astronomical Society of the Pacific* **125**(925), 306–312 (2013) <https://doi.org/10.1086/670067>
- [34] Shakura, N.I., Sunyaev, R.A.: Black holes in binary systems. Observational appearance. *Astronomy and Astrophysics* **24**, 337–355 (1973)

- [35] Tetarenko, B.E., Lasota, J.-P., Heinke, C.O., Dubus, G., Sivakoff, G.R.: Strong disk winds traced throughout outbursts in black-hole X-ray binaries. *Nature* **554**(7690), 69–72 (2018) <https://doi.org/10.1038/nature25159> arXiv:1801.07203 [astro-ph.HE]
- [36] Balbus, S.A., Hawley, J.F.: A Powerful Local Shear Instability in Weakly Magnetized Disks. I. Linear Analysis. *The Astrophysical Journal* **376**, 214 (1991) <https://doi.org/10.1086/170270>
- [37] Balbus, S.A., Hawley, J.F.: Instability, turbulence, and enhanced transport in accretion disks. *Reviews of Modern Physics* **70**(1), 1–53 (1998) <https://doi.org/10.1103/RevModPhys.70.1>
- [38] Hameury, J.-M., Menou, K., Dubus, G., Lasota, J.-P., Hure, J.-M.: Accretion disc outbursts: a new version of an old model. *Monthly Notices of the Royal Astronomical Society* **298**(4), 1048–1060 (1998) <https://doi.org/10.1046/j.1365-8711.1998.01773.x> arXiv:astro-ph/9803242 [astro-ph]
- [39] Lasota, J.-P.: The disc instability model of dwarf novae and low-mass X-ray binary transients. *New Astronomy Reviews* **45**(7), 449–508 (2001) [https://doi.org/10.1016/S1387-6473\(01\)00112-9](https://doi.org/10.1016/S1387-6473(01)00112-9) arXiv:astro-ph/0102072 [astro-ph]
- [40] Meyer, F.: Transition waves in accretion disks. *Astronomy and Astrophysics* **131**(2), 303–308 (1984)
- [41] Vishniac, E.T., Wheeler, J.C.: The Speed of Cooling Fronts and the Functional Form of the Dimensionless Viscosity in Accretion Disks. *The Astrophysical Journal* **471**, 921 (1996) <https://doi.org/10.1086/178019> arXiv:astro-ph/9603159 [astro-ph]
- [42] Dubus, G., Done, C., Tetarenko, B.E., Hameury, J.-M.: The impact of thermal winds on the outburst lightcurves of black hole X-ray binaries. *Astronomy and Astrophysics* **632**, 40 (2019) <https://doi.org/10.1051/0004-6361/201936333> arXiv:1909.13601 [astro-ph.HE]
- [43] Dubus, G., Hameury, J.-M., Lasota, J.-P.: The disc instability model for X-ray transients: Evidence for truncation and irradiation. *Astronomy and Astrophysics* **373**, 251–271 (2001) <https://doi.org/10.1051/0004-6361:20010632> arXiv:astro-ph/0102237 [astro-ph]
- [44] You, B., Cao, X., Yan, Z., Hameury, J.-M., Czerny, B., Wu, Y., Xia, T., Sikora, M., Zhang, S.-N., Du, P., Zycki, P.T.: Observations of a black hole x-ray binary indicate formation of a magnetically arrested disk. *Science* **381**(6661), 961–964 (2023) <https://doi.org/10.1126/science.abo4504> arXiv:2309.00200 [astro-ph.HE]
- [45] Mineshige, S., Osaki, Y.: Disk-instability model for outbursts of dwarf novae. II Full-disk calculations. *Publications of the Astronomical Society of Japan* **37**(1),

- [46] Osaki, Y., Meyer, F., Meyer-Hofmeister, E.: Repetitive rebrightening of EG Cancri: Evidence for viscosity decay in the quiescent disk? *Astronomy and Astrophysics* **370**, 488–495 (2001) <https://doi.org/10.1051/0004-6361:20010234> [arXiv:astro-ph/0102335](https://arxiv.org/abs/astro-ph/0102335) [astro-ph]
- [47] Buat-Ménard, V., Hameury, J.-M.: Superoutbursts, superhumps and the tidal-thermal instability model. *Astronomy and Astrophysics* **386**, 891–898 (2002) <https://doi.org/10.1051/0004-6361:20020307> [arXiv:astro-ph/0202474](https://arxiv.org/abs/astro-ph/0202474) [astro-ph]
- [48] Hameury, J.M.: A review of the disc instability model for dwarf novae, soft X-ray transients and related objects. *Advances in Space Research* **66**(5), 1004–1024 (2020) <https://doi.org/10.1016/j.asr.2019.10.022> [arXiv:1910.01852](https://arxiv.org/abs/1910.01852) [astro-ph.SR]
- [49] You, B., Tuo, Y., Li, C., Wang, W., Zhang, S.-N., Zhang, S., Ge, M., Luo, C., Liu, B., Yuan, W., Dai, Z., Liu, J., Qiao, E., Jin, C., Liu, Z., Czerny, B., Wu, Q., Bu, Q., Cai, C., Cao, X., Chang, Z., Chen, G., Chen, L., Chen, T., Chen, Y., Chen, Y., Chen, Y., Cui, W., Cui, W., Deng, J., Dong, Y., Du, Y., Fu, M., Gao, G., Gao, H., Gao, M., Gu, Y., Guan, J., Guo, C., Han, D., Huang, Y., Huo, J., Jia, S., Jiang, L., Jiang, W., Jin, J., Jin, Y., Kong, L., Li, B., Li, C., Li, G., Li, M., Li, T., Li, W., Li, X., Li, X., Li, X., Li, Y., Li, Z., Liang, X., Liao, J., Liu, C., Liu, G., Liu, H., Liu, X., Liu, Y., Lu, B., Lu, F., Lu, X., Luo, Q., Luo, T., Ma, X., Meng, B., Nang, Y., Nie, J., Ou, G., Qu, J., Sai, N., Shang, R., Song, L., Song, X., Sun, L., Tan, Y., Tao, L., Wang, C., Wang, G., Wang, J., Wang, L., Wang, W., Wang, Y., Wen, X., Wu, B., Wu, B., Wu, M., Xiao, G., Xiao, S., Xiong, S., Xu, Y., Yang, J., Yang, S., Yang, Y., Yi, Q., Yin, Q., You, Y., Zhang, A., Zhang, C., Zhang, F., Zhang, H., Zhang, J., Zhang, T., Zhang, W., Zhang, W., Zhang, W., Zhang, Y., Zhang, Y., Zhang, Y., Zhang, Y., Zhang, Z., Zhang, Z., Zhao, H., Zhao, X., Zheng, S., Zhou, D., Zhou, J., Zhu, Y., Zhu, Y.: Insight-HXMT observations of jet-like corona in a black hole X-ray binary MAXI J1820+070. *Nature Communications* **12**, 1025 (2021) <https://doi.org/10.1038/s41467-021-21169-5> [arXiv:2102.07602](https://arxiv.org/abs/2102.07602) [astro-ph.HE]
- [50] Belloni, T.M., Motta, S.E.: Transient Black Hole Binaries. In: Bambi, C. (ed.) *Astrophysics of Black Holes: From Fundamental Aspects to Latest Developments*. *Astrophysics and Space Science Library*, vol. 440, p. 61 (2016). [https://doi.org/10.1007/978-3-662-52859-4\\_2](https://doi.org/10.1007/978-3-662-52859-4_2)
- [51] Miyamoto, S., Kimura, K., Kitamoto, S., Dotani, T., Ebisawa, K.: X-Ray Variability of GX 339-4 in Its Very High State. *The Astrophysical Journal* **383**, 784 (1991) <https://doi.org/10.1086/170837>
- [52] Arnaud, K.A.: XSPEC: The First Ten Years. In: Jacoby, G.H., Barnes, J. (eds.) *Astronomical Data Analysis Software and Systems V*. *Astronomical Society of the Pacific Conference Series*, vol. 101, p. 17 (1996)
- [53] Wilms, J., Allen, A., McCray, R.: On the Absorption of X-Rays in the Interstellar

- Medium. *The Astrophysical Journal* **542**(2), 914–924 (2000) <https://doi.org/10.1086/317016> [arXiv:astro-ph/0008425](https://arxiv.org/abs/astro-ph/0008425) [astro-ph]
- [54] O’Connor, B., Hare, J., Younes, G., Gendreau, K., Arzoumanian, Z., Ferrara, E.: NICER detection of Swift J1727.8-1613 (GRB 230824A). *The Astronomer’s Telegram* **16207**, 1 (2023)
  - [55] Zdziarski, A.A., Szanecki, M., Poutanen, J., Gierliński, M., Biernacki, P.: Spectral and temporal properties of Compton scattering by mildly relativistic thermal electrons. *Monthly Notices of the Royal Astronomical Society* **492**(4), 5234–5246 (2020) <https://doi.org/10.1093/mnras/staa159> [arXiv:1910.04535](https://arxiv.org/abs/1910.04535) [astro-ph.HE]
  - [56] García, J., Dauser, T., Lohfink, A., Kallman, T.R., Steiner, J.F., McClintock, J.E., Brenneman, L., Wilms, J., Eikmann, W., Reynolds, C.S., Tombesi, F.: Improved Reflection Models of Black Hole Accretion Disks: Treating the Angular Distribution of X-Rays. *The Astrophysical Journal* **782**(2), 76 (2014) <https://doi.org/10.1088/0004-637X/782/2/76> [arXiv:1312.3231](https://arxiv.org/abs/1312.3231) [astro-ph.HE]
  - [57] Dauser, T., García, J., Walton, D.J., Eikmann, W., Kallman, T., McClintock, J., Wilms, J.: Normalizing a relativistic model of X-ray reflection. Definition of the reflection fraction and its implementation in relxill. *Astronomy and Astrophysics* **590**, 76 (2016) <https://doi.org/10.1051/0004-6361/201628135> [arXiv:1601.03771](https://arxiv.org/abs/1601.03771) [astro-ph.HE]
  - [58] Kubota, A., Tanaka, Y., Makishima, K., Ueda, Y., Dotani, T., Inoue, H., Yamaoka, K.: Evidence for a Black Hole in the X-Ray Transient GRS 1009-45. *Publications of the Astronomical Society of Japan* **50**, 667–673 (1998) <https://doi.org/10.1093/pasj/50.6.667>
  - [59] Basak, R., Zdziarski, A.A.: Spectral analysis of the XMM-Newton data of GX 339-4 in the low/hard state: disc truncation and reflection. *Monthly Notices of the Royal Astronomical Society* **458**(2), 2199–2214 (2016) <https://doi.org/10.1093/mnras/stw420> [arXiv:1512.01833](https://arxiv.org/abs/1512.01833) [astro-ph.HE]
  - [60] Shimura, T., Takahara, F.: On the Spectral Hardening Factor of the X-Ray Emission from Accretion Disks in Black Hole Candidates. *The Astrophysical Journal* **445**, 780 (1995) <https://doi.org/10.1086/175740>
  - [61] Pringle, J.E.: The properties of external accretion discs. *Monthly Notices of the Royal Astronomical Society* **248**, 754 (1991) <https://doi.org/10.1093/mnras/248.4.754>
  - [62] Tanaka, T.: Exact time-dependent solutions for the thin accretion disc equation: boundary conditions at finite radius. *Monthly Notices of the Royal Astronomical Society* **410**(2), 1007–1017 (2011) <https://doi.org/10.1111/j.1365-2966.2010.17496.x> [arXiv:1007.4474](https://arxiv.org/abs/1007.4474) [astro-ph.HE]



- [63] King, A.R., Ritter, H.: The light curves of soft X-ray transients. *Monthly Notices of the Royal Astronomical Society* **293**(1), 42–48 (1998) <https://doi.org/10.1046/j.1365-8711.1998.01295.x>
- [64] Lipunova, G.V.: Evolution of Finite Viscous Disks with Time-independent Viscosity. *The Astrophysical Journal* **804**(2), 87 (2015) <https://doi.org/10.1088/0004-637X/804/2/87> [arXiv:1503.09093](https://arxiv.org/abs/1503.09093) [astro-ph.HE]
- [65] Jiang, N., Yang, H., Wang, T., Zhu, J., Lyu, Z., Dou, L., Wang, Y., Wang, J., Pan, Z., Liu, H., Shu, X., Zheng, Z.: Tick-Tock: The Imminent Merger of a Supermassive Black Hole Binary. *arXiv e-prints*, 2201–11633 (2022) <https://doi.org/10.48550/arXiv.2201.11633> [arXiv:2201.11633](https://arxiv.org/abs/2201.11633) [astro-ph.HE]
- [66] Ward, C., Gezari, S., Nugent, P., Kerr, M., Eracleous, M., Frederick, S., Hammerstein, E., Graham, M.J., van Velzen, S., Kasliwal, M.M., Laher, R.R., Masci, F.J., Purdum, J., Racine, B., Smith, R.: Panic at the ISCO: Time-varying Double-peaked Broad Lines from Evolving Accretion Disks Are Common among Optically Variable AGNs. *The Astrophysical Journal* **961**(2), 172 (2024) <https://doi.org/10.3847/1538-4357/ad147d> [arXiv:2309.02516](https://arxiv.org/abs/2309.02516) [astro-ph.GA]
- [67] Yuan, F., Taam, R.E., Misra, R., Wu, X.-B., Xue, Y.: Accretion Disk Spectra of the Brightest Ultraluminous X-Ray Source in M82. *The Astrophysical Journal* **658**(1), 282–287 (2007) <https://doi.org/10.1086/511301> [arXiv:astro-ph/0611939](https://arxiv.org/abs/astro-ph/0611939) [astro-ph]
- [68] Wu, Q., Gu, M.: The X-Ray Spectral Evolution in X-Ray Binaries and Its Application to Constrain the Black Hole Mass of Ultraluminous X-Ray Sources. *The Astrophysical Journal* **682**(1), 212–217 (2008) <https://doi.org/10.1086/588187> [arXiv:0803.2551](https://arxiv.org/abs/0803.2551) [astro-ph]
- [69] Cao, X.-F., Wu, Q., Dong, A.-J.: Different X-Ray Spectral Evolution for Black Hole X-Ray Binaries in Dual Tracks of Radio-X-Ray Correlation. *The Astrophysical Journal* **788**(1), 52 (2014) <https://doi.org/10.1088/0004-637X/788/1/52> [arXiv:1404.5316](https://arxiv.org/abs/1404.5316) [astro-ph.HE]
- [70] Yang, Q.-X., Xie, F.-G., Yuan, F., Zdziarski, A.A., Gierliński, M., Ho, L.C., Yu, Z.: Correlation between the photon index and X-ray luminosity of black hole X-ray binaries and active galactic nuclei: observations and interpretation. *Monthly Notices of the Royal Astronomical Society* **447**(2), 1692–1704 (2015) <https://doi.org/10.1093/mnras/stu2571> [arXiv:1412.1358](https://arxiv.org/abs/1412.1358) [astro-ph.HE]
- [71] Zdziarski, A.A., Poutanen, J., Paciesas, W.S., Wen, L.: Understanding the Long-Term Spectral Variability of Cygnus X-1 with Burst and Transient Source Experiment and All-Sky Monitor Observations. *The Astrophysical Journal* **578**(1), 357–373 (2002) <https://doi.org/10.1086/342402> [arXiv:astro-ph/0204135](https://arxiv.org/abs/astro-ph/0204135) [astro-ph]

- [72] Beloborodov, A.M.: Accretion Disk Models. In: Poutanen, J., Svensson, R. (eds.) High Energy Processes in Accreting Black Holes. Astronomical Society of the Pacific Conference Series, vol. 161, p. 295 (1999). <https://doi.org/10.48550/arXiv.astro-ph/9901108>
- [73] Xie, F.-G., Yuan, F.: Radiative efficiency of hot accretion flows. Monthly Notices of the Royal Astronomical Society **427**(2), 1580–1586 (2012) <https://doi.org/10.1111/j.1365-2966.2012.22030.x> [arXiv:1207.3113](https://arxiv.org/abs/1207.3113) [astro-ph.HE]